J. Fluid Mech. (1976), *vol.* 74, *part* 3, *pp.* 477–495
Printed in Great Britain

Oxygen vibrational and dissociation relaxation behind regular reflected shocks

By H. OERTEL, JR
Institut für Strömungslehre und Strömungsmaschinen, Universität Karlsruhe, Germany

(Received 24 June 1975)

The oxygen vibrational and dissociation relaxation behind regular reflected shocks has been calculated and measured. Numerical calculations using published rate coefficients supplied the relaxation-zone data needed to estimate the range of most useful experimental conditions. Then photographs of the shock reflexion were taken using a complementary double-exposure interferometer. The density profiles in the relaxation zones behind the reflected shocks were measured by means of a multibeam laser–differential interferometer. The results of these experiments confirmed the theoretical model adopted for the calculations within a certain range of experimental conditions, but clearly revealed the need for revising the rate coefficients. New calculations with different vibrational relaxation times and dissociation rate coefficients then had the result that the best fit of calculated to measured profiles was obtained when the following values were inserted.

Vibration

$$p\tau_v = A_v \exp(B_v T^{-\frac{1}{3}}),$$
$$A_v = (2{\cdot}1 \pm 0{\cdot}2) \times 10^{-5}\ \text{kg/ms}, \quad B_v = 129\ ^\circ\text{K}^{\frac{1}{3}}.$$

Dissociation: $O_2 + O_2 \rightleftharpoons 2O + O_2$

$$\overrightarrow{k_1} = A_1 T^{-2{\cdot}5} \exp(-\theta_D/T),$$
$$A_1 = (6{\cdot}2 \pm 0{\cdot}5) \times 10^{18}\ \text{m}^3\ ^\circ\text{K}^{2{\cdot}5}/\text{mol s}, \quad \theta_D = 59136\ ^\circ\text{K}.$$

Dissociation: $O_2 + O \rightleftharpoons 3O$

$$\overrightarrow{k_2} = A_2 T^{-1{\cdot}0} \exp(-\theta_D/T),$$
$$A_2 = (4{\cdot}0 \mp 0{\cdot}5) \times 10^{13}\ \text{m}^3\ ^\circ\text{K/mol s}.$$

1. Introduction

Oxygen vibrational and dissociation relaxation has been extensively studied since 1956 in shock tubes behind normal shocks. For instance Blackman (1956) and White & Millikan (1963) measured the vibrational relaxation. Byron (1959), Camac & Vaughan (1961), Mathews (1959) and Stricker & Low (1972) investigated the dissociation relaxation. There have also been a few experiments with nozzle flows, bow waves of wedges, cones, spheres and cylinders as well as within

expansions following shock compression. The results have been compiled and discussed in the books or reviews of Bortner & Golden (1961), Bradley (1962), Camac & Feinberg (1967), Clarke & McChesney (1964), Gaydon & Hurle (1963), Hall & Russo (1967), Jalbert (1966), Oertel (1966), Stupochenko, Losev & Osipov (1967), Vincenti & Kruger (1965), Wecken (1968) and Zel'dovich & Raizer (1967). The oxygen vibrational relaxation times proposed by different authors agree well within experimental uncertainty, but the dissociation rates at high temperatures differ by more than a factor of ten. Thus it seemed worth while to redetermine these by means of another gasdynamic phenomenon and by using new measuring and evaluation techniques.

Having compared calculated relaxation zones behind incident and reflected shocks we concluded that investigation of relaxation behind regular reflected shocks would be a good method. The temperature variation during relaxation is smaller than that encountered behind an incident shock with the same final equilibrium temperature. It can be varied by simply changing the wedge angle. High degrees of dissociation can be obtained in a simple shock tube without heating the driver gas. On the other hand there was some doubt if these obvious advantages could be realized within the 15 cm shock tube at our disposal. It was possible that combined molecular transport and relaxation near the reflexion point as well as the overlapping region of the relaxation zones behind the incident and reflected shocks could not be neglected. These problems are the first to be treated by numerical calculations and experiments. Photographs of the shock configuration have been taken and density profiles of the relaxation zones have been measured by means of laser–differential interferometers. Recalculations with different relaxation coefficients have been performed until the theoretical density profiles fitted all the experimental ones.

2. Theory

2.1. *Basic equations*

Figure 1 shows the regular shock configuration, assumed to be stationary in the moving frame of the reflexion point P. The gas enters the oblique shock I having shock angle α_1, with flow velocity u_1 and in thermodynamic equilibrium state (1). After having passed through the first hatched relaxation zone it reaches equilibrium state (2) and has then turned through the deflexion angle β_2. The gas then enters the oblique shock R with velocity u_2 and in state (2). Having passed through the second hatched relaxation zone it finally reaches equilibrium state (3) and a flow velocity u_3, which is assumed to be parallel to the wall:

$$\beta_2 = \beta_3. \tag{2.1}$$

This means that we completely neglect the overlapping region of the relaxation zones of the incident and reflected shock as well as boundary-layer effects. We also neglect viscosity, diffusion and heat conduction within the relaxation zones far from the wall. Theoretical work of Arkhipov & Polenov (1969), Gibson & Buckmaster (1964), Wassner (1972) and Weihs & Gal-Or (1972) has confirmed that this is correct within the temperature range of our experiments. With these

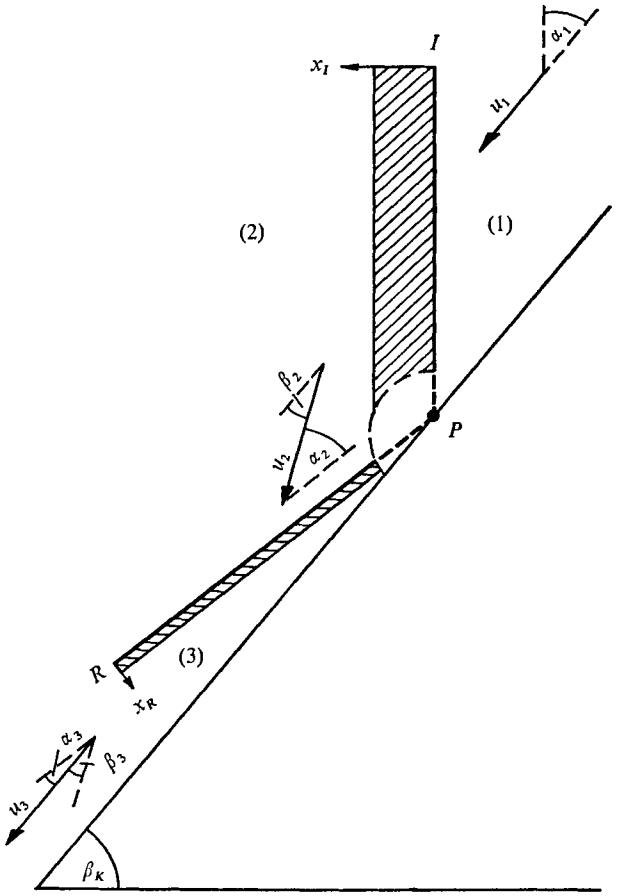

FIGURE 1. Sketch of regular shock reflexion.

assumptions the *balance equations* for mass, momentum and energy for the normal components of the velocities u_n are

$$\rho u_n = K, \quad p + \rho u_n^2 = P, \tag{2.2), (2.3}$$

$$h + \tfrac{1}{2}u_n^2 = H, \tag{2.4}$$

with K, P and H constants. h is the specific enthalpy, p denotes pressure and ρ density. We use (2.1)–(2.4) to calculate the equilibrium states (2) and (3), the frozen states ($2f$) and $3f$), in which the relaxation variable has the value ahead of the shock, as well as the relaxation zones of the incident and reflected shock.

The caloric *equation of state* adopted is given by the following formulae, assuming rigid rotators, harmonic oscillators and factorized partition functions:

$$h = \frac{(5+\alpha_D)}{2} RT + \alpha_D(R\theta_D + e_{el}^{O}) + (1-\alpha_D)(e_v + e_{el}^{O_2}) + \frac{p}{\rho}, \tag{2.5}$$

$$\frac{\alpha_D^2}{1-\alpha_D} = \frac{m^{O}}{2\rho V} \frac{(Z^{O})^2}{Z^{O_2}} \exp\left(-\frac{\theta_D}{T}\right), \tag{2.6}$$

$$e_v = \frac{R\theta_v}{\exp(\theta_v/T) - 1}. \tag{2.7}$$

e_v is the specific energy of vibration and α_D the degree of dissociation. θ_v and θ_D denote the characteristic temperatures for vibration and dissociation, R the gas constant for the molecular gas, m^O the mass of the oxygen atom and Z^O, Z^{O_2}, e_{el}^O and $e_{el}^{O_2}$ the partition functions and specific electron energies of the oxygen atoms and molecules. For the numerical calculations we used the same values as Law (1970).

The thermal equation of state of dissociated gas is

$$p = (1+\alpha_D) R\rho T, \tag{2.8}$$

with T the temperature.

Within the relaxation zones we assume the specific enthalpy h to be a function of p, ρ and only one relaxation variable e_v or α_D. The calculations of Bray (1959), Maillie & Hsu (1968) and Taylor (1966) confirm that this is correct for our experimental conditions. We use the following vibrational *relaxation equation*:

$$de_v/dt = (e_{v_e} - e_v)/\tau_v. \tag{2.9}$$

e_{v_e} is the equilibrium specific vibrational energy at the translation temperature T and τ_v denotes the vibrational relaxation time. We use the simplified Landau & Teller (1936) assumption:

$$p\tau_v = A_v \exp(B_v T^{-\frac{1}{3}}). \tag{2.10}$$

For the preliminary calculations preparing the experiments the Millikan & White (1963) values of A_v and B_v have been inserted.

Within the dissociation relaxation zone the following two reaction pairs have been considered:

$$O_2 + O_2 \underset{}{\overset{\vec{k}_1}{\rightleftharpoons}} 2O + O_2,$$

$$O_2 + O \underset{}{\overset{\vec{k}_2}{\rightleftharpoons}} 3O,$$

with dissociation rates $\vec{k}_1$ and $\vec{k}_2$.

The relaxation equation

$$\frac{d\alpha_D}{dt} = \frac{\rho}{\mathcal{M}_{O_2}} (\vec{k}_1(1-\alpha_D) + 2\vec{k}_2\alpha_D) \frac{(1-\alpha_D)\alpha_e^2 - (1-\alpha_e)\alpha_D^2}{\alpha_e^2} \tag{2.11}$$

is based upon the assumption that the ratios of the dissociation and recombination rates are equal to the equilibrium constant. α_e is the equilibrium degree of dissociation at the translation temperature T. The temperature dependence of the dissociation rate coefficients has been assumed to be

$$\vec{k}_1 = A_1 T^{B_1} \exp(-\theta_D/T), \quad \vec{k}_2 = A_2 T^{B_2} \exp(-\theta_D/T). \tag{2.12}$$

For the preliminary calculations preparing the experiments Millikan & White's (1963) values of A_1, A_2, B_1 and B_2 have been used.

2.2. *Numerical calculations*

Four different calculations have been performed.

(i) Calculation preparing the experiments using published relaxation coefficients from Millikan & White (1963), Mathews (1959) and Wray (1963) and using the theoretical boundary condition (2.1).

1	1——2*f*——2*e*——2——3*f*——3*e*——3
2	1——2*f*——2*e*————3*f*——3*e*——3
3	1——2*f*——2*e*————3*f*——3*e*——
4	1——2*f*————————3*f*——3*e*——

TABLE 1. Theoretical models

(ii) Evaluation of the measured density profiles of the relaxation zones with various vibrational relaxation times (2.10) and dissociation rate coefficients (2.12) using measured reflexion angles α_3 and not the theoretical boundary condition (2.1).

(iii) Calculation of the density profiles using measured reflexion angles α_3 and the new dissociation rates found by calculation (ii).

(iv) Repeat of calculation (i) using the theoretical boundary condition (2.1) and the new dissociation rates. Some results of these calculations are given in this section.

The results of (ii) and (iii) are presented in §4.

The theoretical models presented in table 1 have been used to calculate the relaxation zones behind the incident and reflected shock. States (*f*) are without vibrational energy and any degree of dissociation. States (*e*) are intermediate ones with equilibrium vibration and frozen dissociation. States (2) and (3) are the equilibrium states well downstream of the relaxation zones. Outside the region where the relaxation zones overlap model 1 may be realized. The molecules pass through the vibrational and dissociation relaxation zones of the incident shock and reach equilibrium state (2). Via the vibrational and dissociation relaxation zones of the reflected shock they finally reach equilibrium state (3). Model 2 may be appropriate if the dissociation relaxation zone behind the incident shock is so long that the vibration is in equilibrium while the dissociation stays practically frozen. Model 3 neglects dissociation and may be correct at moderate shock Mach numbers. If the vibrational relaxation zone behind the incident shock is then quite long model 4 may be applied.

In figure 2 the critical incidence angle α_{Gr} is plotted as function of the incident shock Mach number $M_S = M_1 \sin\alpha_1$. Only at incidence angles smaller than α_{Gr} does regular shock reflexion occur. At angles larger than α_{Gr} Mach reflexion occurs. This diagram reveals an important limitation on possible experimental conditions. The dashed line represents the well-known perfect-gas result. The dash–dot line has been calculated taking into consideration the oxygen vibration. The solid lines are from the equation of state (2.5) at several initial pressures p_1. The vibration has some influence at shock Mach numbers higher than 1·5. Perceptible dissociation starts at a Mach number of 4·3 and strongly increases the critical incidence angle. For instance, at a shock Mach number of 10 and initial pressure of 133 N/m^2, α_{Gr} rises to 49·2° compared with 42·8° for harmonic vibration only and compared with 39·9° for a perfect gas. The difference is quite remarkable and demonstrates the strong dissociation effect.

Figure 3 presents the ratio x_I/x_R of the lengths of the relaxation zones behind the incident and reflected shock, defined as the normal distance at which the

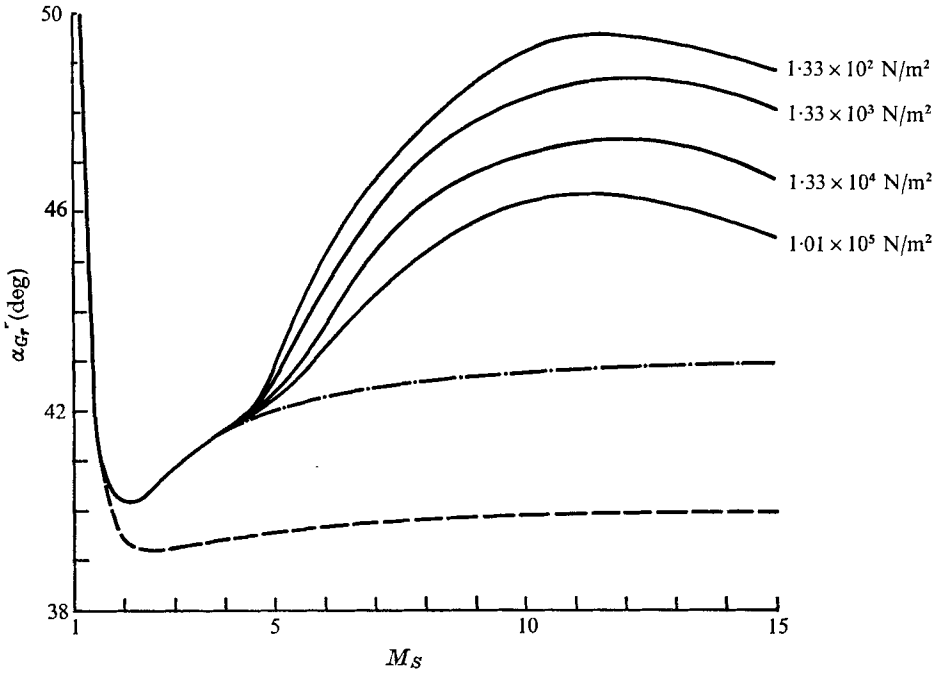

FIGURE 2. Critical incidence angle α_{Gr}. $T_1 = 293$ °K (1 Torr = 133·32 N/m²). – – –, perfect gas; —·—, vibration; ——, dissociation.

relaxation variable e_v or α_D has reached 90 % of its equilibrium value. We see a ratio of 100 of the dissociation relaxation lengths at a shock Mach number $M_S = 9$. This means that quite a large range of conditions may exist where the reflected shock runs into the frozen state behind the incident shock, frozen with respect to dissociation. This yields the important result that theoretical model 2 corresponds to reality. The ratio of the length of the vibrational relaxation zone behind the incident shock and the dissociation relaxation zone behind the reflected shock is only 0·6 at a shock Mach number of 9. For this reason model 2 is a good one when calculating dissociation relaxation behind the reflected shock.

The ratio of vibrational relaxation lengths is 21 at a Mach number of 6. Within a large range of experimental conditions the reflected shock also runs into the frozen state behind the incident shock, frozen with respect to vibration. Theoretical model 4 can be used for calculating the vibrational relaxation behind the reflected shock.

In figures 4 and 5 the 50, 90 and 99 % lengths of the vibrational and dissociation relaxation zones behind the reflected shock are plotted as functions of shock Mach number M_S. For example, the vibrational relaxation zone has a length of 3 mm at $M_S = 6$ and the dissociation relaxation zone a length of 6 mm at $M_S = 9$.

Other important results of the calculations clearly revealed the advantages of investigating relaxation behind regular reflected shocks. The equilibrium temperature behind the reflected shock amounts to 3560 °K at an incident shock

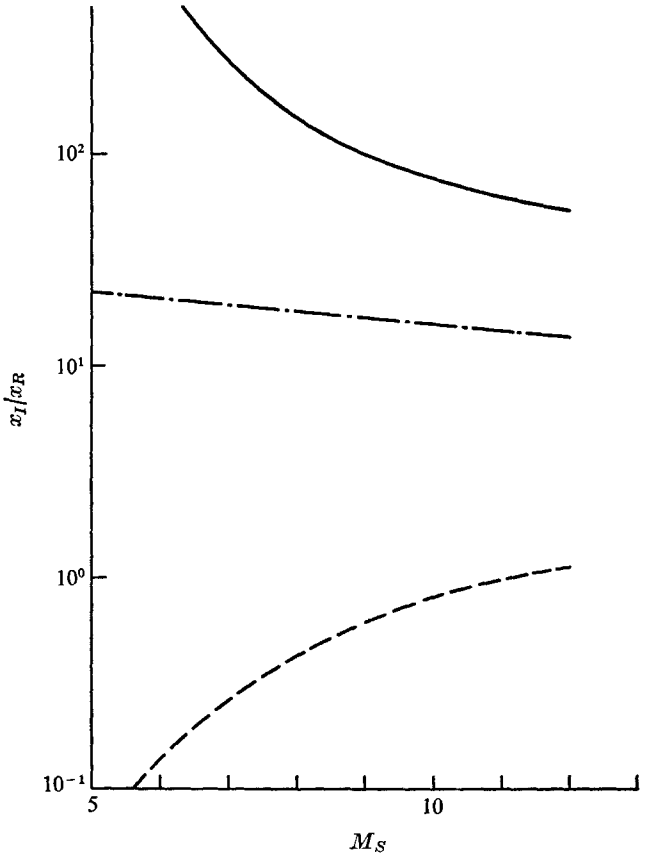

FIGURE 3. Ratio of lengths of relaxation zones behind the incident and reflected shock. ——, model 1; – – –, model 2; —·—, model 3. $p_1 = 133$ N/m^2, $\beta_K = 60°$, $T_1 = 293$ °K.

Mach number of 9. Producing the same equilibrium temperature behind the incident shock under the same initial conditions needs a shock Mach number as high as 14·6, which can be obtained only in a shock tube with a heated driver gas. An even more important advantage is that the temperature variation during relaxation is smaller than that encountered with the same equilibrium temperature behind the incident shock. For instance, in the case of an equilibrium temperature of 3560 °K, the difference between the translation temperatures in the frozen and equilibrium state amounts to 5000 °K behind the incident shock compared with only 2000 °K behind the reflected shock. High temperature variations within the relaxation zone have been one of the main sources of error when determining rate coefficients.

We now summarize these results of numerical calculation.

(i) The possible advantage of investigating the relaxation zone behind a regular reflected shock has been quantified.

(ii) The reflected shock runs into the frozen state behind the incident shock. Evaluation of the experiments can rely upon theoretical model 2 for dissociation. Model 4 is adequate for vibration.

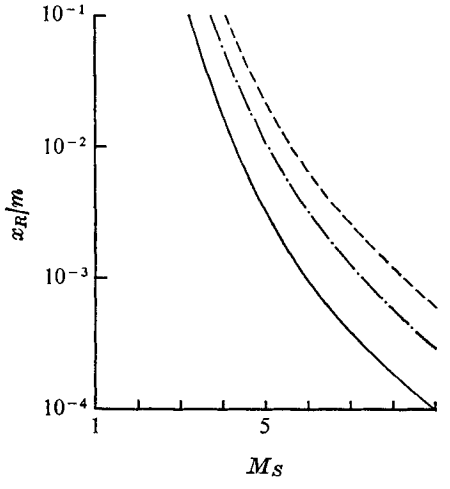

FIGURE 4

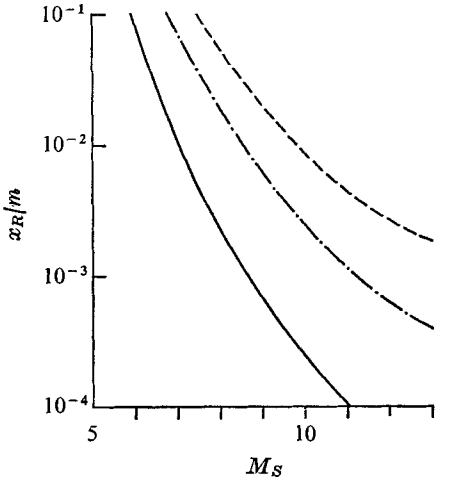

FIGURE 5

FIGURE 4. Length of vibrational relaxation zone behind the reflected shock. Model 4; $p_1 = 133$ N/m², $\beta_K = 60°$, $T_1 = 293$ °K. ——, 50 % of equilibrium; —·—, 90 % of equilibrium; – – –, 99 % of equilibrium.

FIGURE 5. Length of dissociation relaxation zone behind the reflected shock. Model 2; data and curves as in figure 4.

	Vibrational relaxation	Dissociation relaxation
M_S	5–6·5	7–10
p_1 (N/m²)	133–399	133–399
β_K	60°–70°	50°–70°

TABLE 2. Experimental conditions

(iii) The experimental conditions can be chosen such that the extent of the region of overlap of the relevant relaxation zones behind the incident and reflected shock is small.

(iv) The critical incidence angle is strongly affected by vibration and dissociation.

On the basis of these results the ranges of the shock Mach number M_S, initial pressure p_1 and wedge angle β_K in table 2 have been chosen for the experiments. The experiments set out to prove that the hypotheses adopted are adequate.

3. Experiments

3.1. *Facility*

The University of Karlsruhe's low pressure shock tube, which has a total length of 12·5 m and a diameter of 15 cm, was used. Hydrogen at initial pressures of 1–10 bars served as the driver gas. The test gas was high-purity oxygen with initial pressures of 1–3 Torr. The highest shock Mach number obtained was

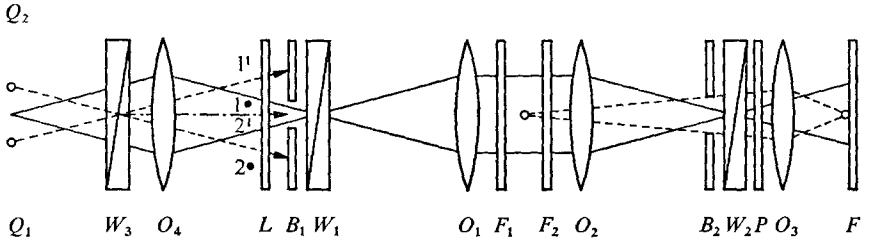

FIGURE 6. Double-exposure differential interferometer.

$M_S = 9{\cdot}5$. Part of the shock wave penetrated into a 9×9 cm tube of rectangular cross-section and was then reflected from a wedge fixed between windows 11 cm in diameter.

3.2. *Shock configurations*

Shock configurations at different wedge angles were visualized by complementary double-exposure interferography. The differential interferometer described by Smeets & George (1972) was employed. The optical set-up is sketched in figure 6. The differential interferometer consists of two Wollaston prisms W_1 and W_2, two objectives O_1 and O_2, the polarizer P and the camera objective O_3, giving an image of the test section through windows F_1 and F_2 on the film F. At its entrance two spark light sources Q_1 and Q_2 of effective duration $0{\cdot}2\ \mu$s, the Wollaston prism W_3, the $\frac{1}{4}\lambda$ plate L and the diaphragm B_1 were used to produce two light beams of opposite circular polarization. The double exposure with light of opposite circular polarization compensates optical faults, which otherwise would distort the quality of the pictures at infinite fringe spacing needed to visualize the low density flow.

Figure 7 (plate 1) presents three typical interferograms visualizing the shock reflexion at incident shock Mach numbers $M_S = 6{\cdot}5$ and $9{\cdot}2$. The time between the two sparks was less than $2\ \mu$s. At $M_S = 9{\cdot}2$ we have vibrational relaxation behind the incident shock and dissociation relaxation behind the reflected shock. The interferograms clearly show that the reflected shock is straight in spite of the relaxation and transport phenomena within the wall boundary layer. The shock is also straight in the region of overlap of the two relaxation zones. This means that the basic assumption of our theoretical model was fulfilled. The same is true at $M_S = 6{\cdot}5$, where we have only vibrational relaxation behind the reflected shock. Many interferograms of this kind confirmed this fact.

The experimental reflexion angles α_3 taken from such interferograms are found to be up to 15% larger than those calculated with the theoretical boundary condition (2.1) assuming equilibrium flow parallel to the wall. This may be due to the combined viscous and entropy-layer displacement effect. We concluded that we should evaluate our measured density profiles with the measured reflexion angles and not with the calculated ones.

3.3. *Density profiles*

The density profiles in the relaxation zones behind the incident and reflected shock were measured by means of four laser–differential interferometers described by Smeets & George (1971), two of which are sketched in figure 8.

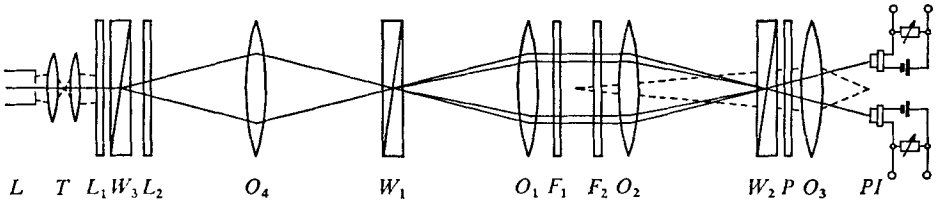

FIGURE 8. Laser–differential interferometer.

The optical arrangement is similar to that in figure 6, but a 15 mW He–Ne laser is now used as the light source. PIN-diodes served as detectors, their signals being recorded by means of oscilloscopes. The laser–differential interferometers had a space resolution of 0·2 mm and a time resolution of 0·1 μs. The simultaneous use of four interferometers made it possible to measure the speed of the incident shock, the reflexion angle α_3 and two density profiles in the relaxation zone behind the reflected shock in each experiment. In this way it could be proved that the regular shock reflexion was stationary in the moving frame and that the relaxation zones were one-dimensional. The speed of the incident shock, the reflexion angle and the state of the gas ahead of the incident shock were used as the input data when calculating the equilibrium states behind the incident and reflected shock.

The signal given by one of the interferometers and the density profile evaluated from this are shown in figure 9. The experimental conditions were such that vibrational relaxation occurred behind the incident shock (signal marked I) and dissociation relaxation behind the reflected shock (signal marked R). The signal clearly shows the decay of the density gradient in both relaxation zones with increasing time. I_0 denotes maximum light intensity. Equilibrium states are indicated by $\bar{I}$.

The light intensities $I(t)$, given by the PIN-diodes in terms of density, were evaluated using the following formula:

$$I = I_0 \cos^2(\pi/\lambda_0^{-1}\Gamma). \tag{3.1}$$

Γ denotes the optical path difference between the two interfering beams 1 and 2 at the vacuum wavelength λ_0. Γ is the sum of $\bar{\Gamma}$, produced by the Wollaston prisms, and $\Delta\Gamma$, due to the refraction-index difference Δn in the test section of width S:

$$\Delta\Gamma = \Gamma - \bar{\Gamma} = S\Delta n. \tag{3.2}$$

The refraction index n is related to the density ρ by

$$n - 1 = G_{O_2}(1-\alpha_D)\rho + G_O\alpha_D\rho. \tag{3.3}$$

G_O and G_{O_2} are the Gladstone–Dale constants of oxygen atoms and molecules. The values given by Wettlaufer (1969) have been used.

When evaluating density the following difficulty had to be overcome. Up to the mark R_D in figure 9(*b*) the density due to the reflected shock and within the relaxation zone is measured directly because the shock runs between the two interfering light beams as shown in figure 9(*a*). The density rise is so high that $\Delta\Gamma$ rises above λ_0 and the signal becomes ambiguous. As soon as the shock has

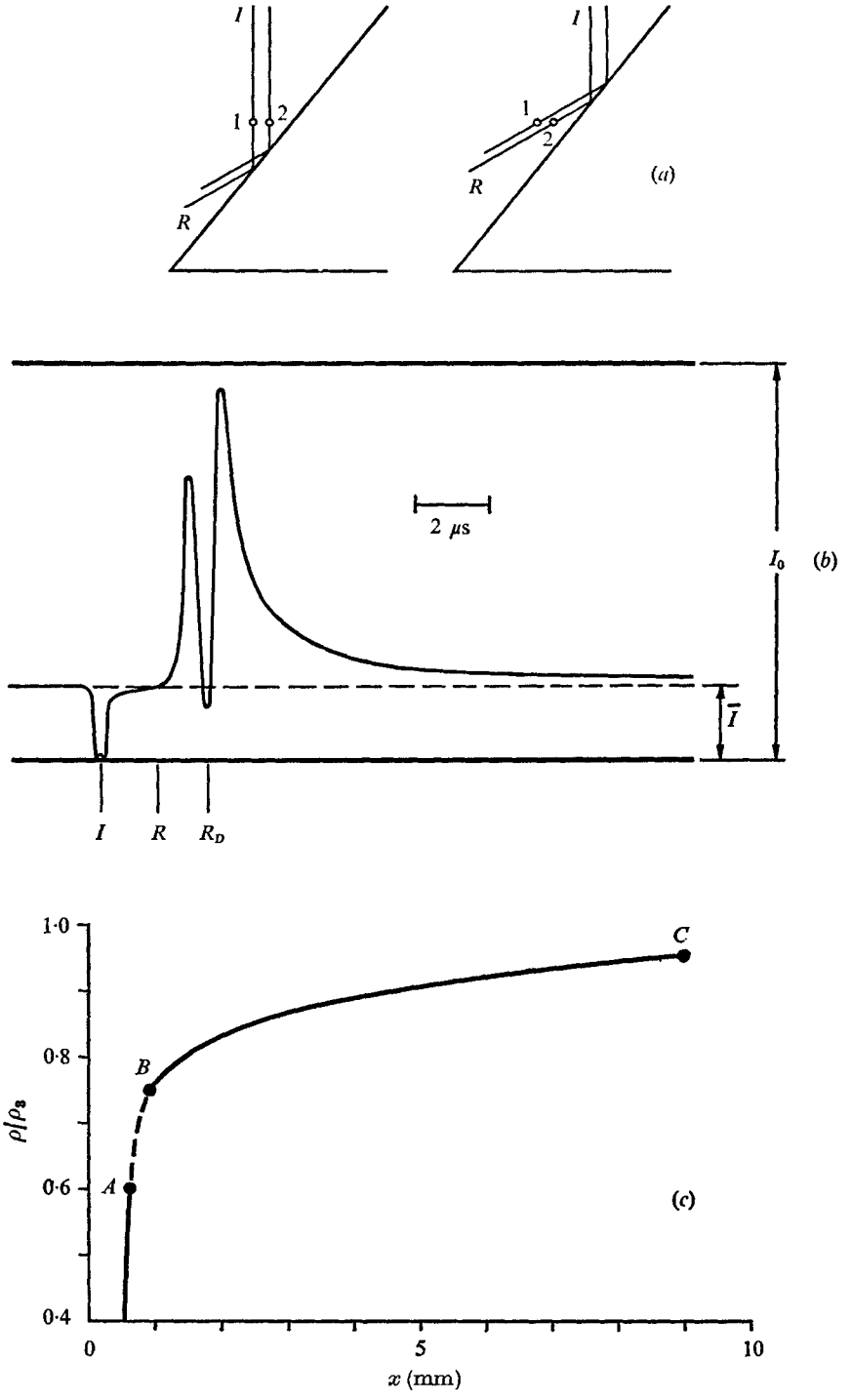

FIGURE 9. Signal and evaluated density profile. $M_S = 8{\cdot}1$, $p_1 = 137$ N/m², $\beta_K = 60°$, $\alpha_3 = 7{\cdot}2°$, $T_1 = 295$ °K.

passed the second laser beam $\Delta\Gamma$ indicates the density difference between the two beams. The sudden jump in the signal to a lower value is obscured by the finite response time of about 0·1 μs. In order to avoid errors introduced by this the evaluation was based upon the given density ahead of the shock and the calculated density at the end of the useful signal.

Figure 9(*c*) presents the density profile referred to the calculated equilibrium density ρ_3 behind the reflected shock as a function of the normal shock distance x. Up to point A the density is measured directly. Between A and B the density is not known. Between B and C the plotted density profile is evaluated from measured density differences. The measurements were repeated with different gradient sensitivities and different locations of points A and B. The agreement was quite good, and in this way the density profile could be confirmed from the beginning to the end. The maximum error in the measured density rise in the relaxation zone was about 6 % and the deviation from one experiment to another under the same experimental conditions was less than 2 %.

In this manner we have evaluated numerous oscillograms of the vibrational and dissociation relaxation zones behind the regular reflected shock taken under 23 different sets of experimental conditions. The results are presented and the evaluation of the vibrational relaxation time and the dissociation rates is explained in the next section.

4. Evaluation of relaxation coefficients

4.1. *Vibrational relaxation time*

In order to compare the experimental results with theory we calculated the vibrational relaxation zone behind the reflected shock using the relaxation time (2.10) with different constants A_v and B_v published by different authors for all initial conditions studied. The calculations were made using the measured reflexion angles α_3. We approximated the experimental density profiles by analytical functions with a least-squares fit of 1 ‰ accuracy. The comparison of the calculated and measured profiles revealed that the best agreement is obtained with the relaxation constants of Millikan & White (1963). In particular, the values of Blackman (1956) do not fit our experimental results.

Figure 10 presents two examples. The density ρ referred to the calculated density ρ_3 behind the reflected shock is plotted as function of the shock distance x. It can be seen that the theoretical and experimental density profiles agree within the experimental error. The gap in the experimental density curve is due to the above-mentioned distorted part of the signal. At the beginning of the relaxation zones some discrepancies can be seen. These can be explained by the shock structure where translation and rotation of the oxygen molecules comes into equilibrium. Our theoretical model assumed a frozen state at $x = 0$, with translation and rotation in thermodynamic equilibrium. Therefore the density profile measured in the first 0·3 mm is not compatible with our model. This part of the profile was excluded from comparison. Also, for all other measured density profiles the agreement between the experimental and theoretical vibrational relaxation zones was just as good. The oxygen vibrational relaxation times of

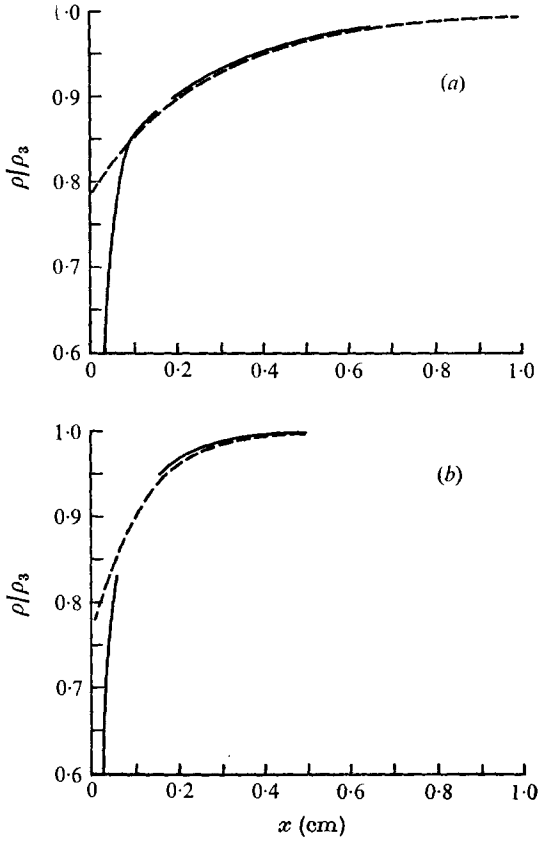

FIGURE 10. Vibrational relaxation zone behind the reflected shock. $p_1 = 136\,\mathrm{N/m^2}, \beta_K = 60°$, $T_1 = 295\,°\mathrm{K}$. (*a*) $M_S = 5{\cdot}4$, $\alpha_3 = 11{\cdot}5°$. (*b*) $M_S = 6{\cdot}3$, $\alpha_3 = 9{\cdot}9°$. – – –, theory; ——, experiment.

Millikan & White have been confirmed in the temperature range 2800–4300 °K with the following uncertainty estimated from experimental errors:

$$p\tau_v = A_v \exp(B_v T^{-\frac{1}{3}}),$$

$$A_v = (2{\cdot}1 \pm 0{\cdot}2) \times 10^{-5}\,\mathrm{kg/ms}, \quad B_v = 129\,°\mathrm{K}^{\frac{1}{3}}.$$

The oxygen vibrational relaxation has often been examined and is generally considered to be well known. The fact that our results agree with those published by Millikan & White (1963) supports our theoretical model and gives confidence in our method of investigating relaxation behind regular reflected shocks.

4.2. *Dissociation rate coefficients*

In the same way we have evaluated the dissociation relaxation zones behind regular reflected shocks. We calculated the relaxation zones using the different published reaction rate coefficients $\vec{k}_1$ and $\vec{k}_2$ and the measured reflexion angles α_3. We compared these with the experimental ones. There was no set of dissociation rates that described our experimental results sufficiently well for all

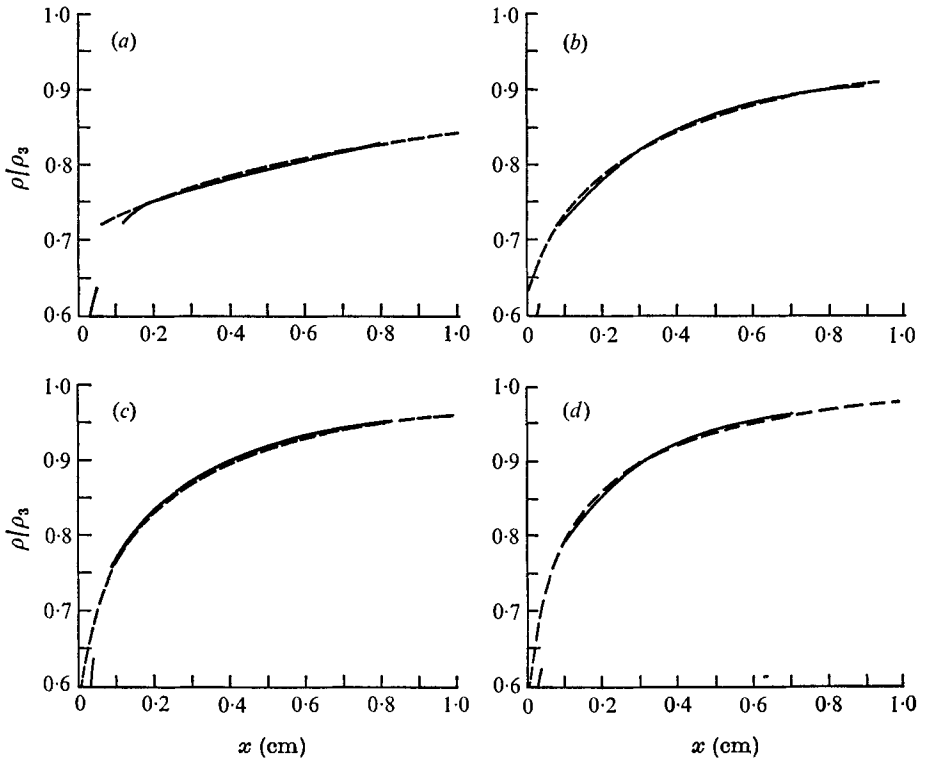

FIGURE 11. Density profiles in the dissociation relaxation behind the reflected shock. $p_1 = 137\,\mathrm{N/m^2}$, $\beta_K = 60°$ or $70°$, $T_1 = 295°\,\mathrm{K}$. (*a*) $M_S = 6{\cdot}95$, $\alpha_3 = 8{\cdot}7°$. (*b*) $M_S = 8{\cdot}1$, $\alpha_3 = 7{\cdot}2°$. (*c*) $M_S = 8{\cdot}9$, $\alpha_3 = 6{\cdot}5°$. (*d*) $M_S = 8{\cdot}8$, $\alpha_3 = 3{\cdot}75°$. ——·——, theory; ——, experiment.

experimental conditions. This means that a redetermination of the oxygen dissociation rates was needed using numerical fitting.

The fitting procedure used was as follows. The experimental density profiles in the dissociation relaxation zone were approximated by a sum of exponential functions through a least-squares fit giving deviations not exceeding 1‰. For all experimental conditions we then calculated the theoretical profiles, inserting various constants A_1 and A_2 for different pairs of B_1 and B_2 into the reaction rate expressions (2.12). The fit was considered to be good if for all experimental conditions the least-squares deviation between the measured and calculated profiles was less than the experimental error.

The results of four such numerical fits are shown in figure 11. The density ρ referred to the calculated equilibrium density ρ_3 behind the reflected shock is plotted as function of the normal shock distance x. It can be seen that the experimental and theoretical density profiles in the dissociation relaxation zone with the new dissociation rates agree very well for all experimental conditions shown. At the beginning of the relaxation zones we see some discrepancy. This is due to the vibrational relaxation zone behind the reflected shock being in agreement with the calculated one (model 3). Doing the calculations with theoretical model

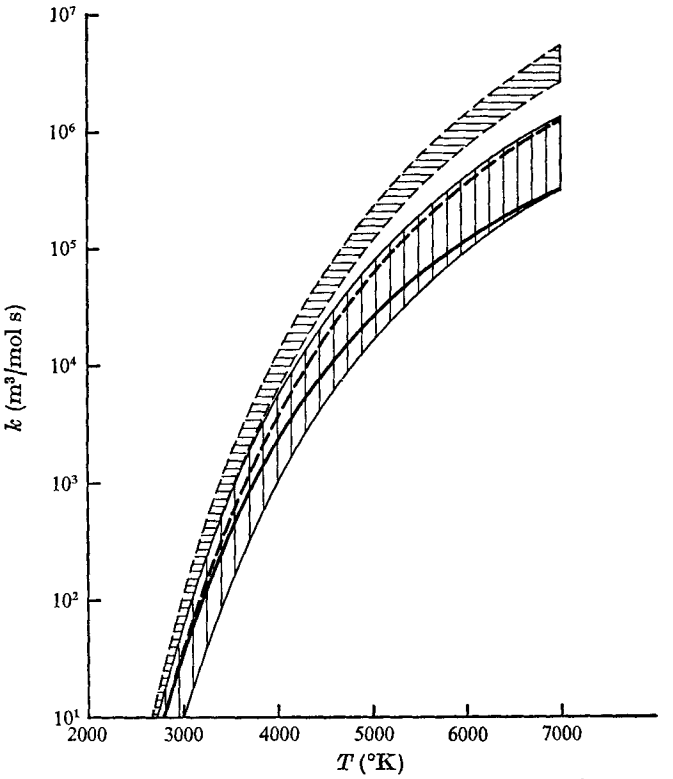

FIGURE 12. Dissociation rate coefficients. ——, $\vec{k_1}$; – – –, $\vec{k_2}$.

2 of table 1 means that we assumed a frozen state at the beginning of the relaxation zone with molecular translation, rotation and vibration in equilibrium and dissociation frozen. The measured density profile in the first 0·2–0·5 mm therefore cannot be compatible with our theoretical model. This part of the experimental profile was excluded from fitting. All other profiles measured under 18 different sets of experimental conditions agreed as well with the theoretical ones which we calculated with the new dissociation rates. The result of the evaluation of the oxygen dissociation rates in the temperature range 3100–7000 °K is the following:

$$O_2+O_2 \rightleftharpoons 2O+O_2, \quad \vec{k_1} = A_1 T^{-2\cdot5} \exp(-\theta_D/T),$$

$$O_2+O \rightleftharpoons 3O, \quad \vec{k_2} = A_2 T^{-1\cdot0} \exp(-\theta_D/T),$$

$$A_1 = (6\cdot2 \pm 0\cdot5) \times 10^{18} \text{ m}^3 \text{ °K}^{2\cdot5}/\text{mol s}, \quad A_2 = (4\cdot0 \mp 0\cdot5) \times 10^{13} \text{ m}^3 \text{ °K/mol s}.$$

The indicated deviations of $\pm 0\cdot5$ and $\mp 0\cdot5$ come from the experimental errors. Within this range positive deviation of $\vec{k_1}$ can be compensated by negative deviation of $\vec{k_2}$.

The values of the new dissociation rate coefficients are now to be compared with those published previously by other authors. All constants in the dissociation rates compiled in table 3 have been considered. Figure 12 presents the

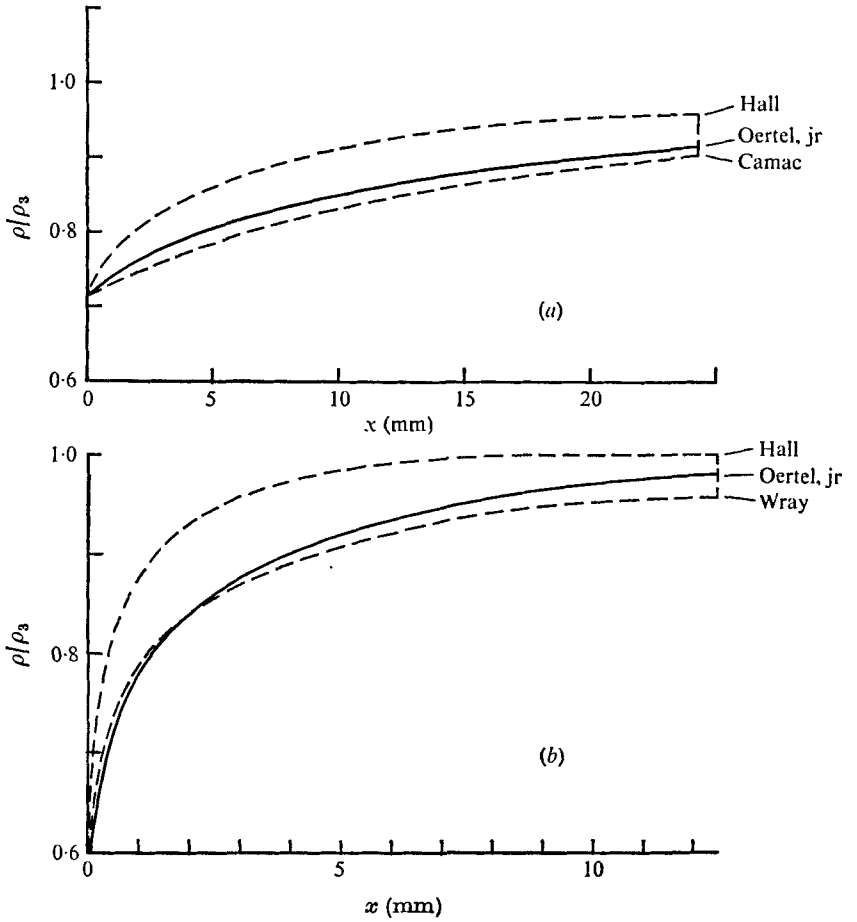

FIGURE 13. Dissociation relaxation zone behind the reflected shock. $p_1 = 133$ N/m^2, $\beta_K = 60°$, $T_1 = 295$ °K. (*a*) $M_S = 6{\cdot}95$, $\alpha_3 = 8{\cdot}7°$. (*b*) $M_S = 8{\cdot}9$, $\alpha_3 = 6{\cdot}5°$.

Author(s)	A_1	B_1	A_2	B_2
Mathews (1959), Wray (1963)	1·1 +19	−2·5	9·0 +13	−1·0
Byron (1959)	1·9 +15	−1·5	1·12+12	−0·5
Hall & Russo (1967)	3·6 +15	−1·5	2·1 +12	−0·5
Camac & Feinberg (1967)	3·25+13	−1·0	9·0 +13	−1·0
Camac & Vaughan (1961)	1·0 +13	−1·0	6·3 +17	−2·0
Martin (1966)	2·3 +13	−1·0	9·0 +13	−1·0
Wray (1963)	3·0 +13	−1·0	9·0 +13	−1·0
Bortner & Golden (1961)	5·5 +11	−0·5	1·83+12	−0·5
Oertel jr (1974)	6·2 +18	−2·5	4·0 +13	−1·0

$$O_2 + O_2 \rightharpoonup O_2 + 2O: \quad \vec{k_1} = A_1 T^{B_1} \exp(-\theta_D/T)$$

$$O_2 + O \rightharpoonup 3O: \quad \vec{k_2} = A_2 T^{B_2} \exp(-\theta_D/T)$$

TABLE 3. Constants in dissociation rates

results as a plot of the dissociation rates $\overrightarrow{k_1}$ and $\overrightarrow{k_2}$ as functions of temperature T. The published values of the dissociation rates are within the hatched areas. The heavy lines represent the new dissociation rate coefficients. The dissociation rates $\overrightarrow{k_1}$ remain within the hatched area but approach its upper edge at high temperatures. The new dissociation rates $\overrightarrow{k_2}$ are significantly smaller than those assumed to date.

The discrepancies between the density profiles in dissociation relaxation zones behind regular reflected shocks calculated with previously adopted and the new rate coefficients are displayed in figure 13. The dashed density profiles were calculated using the dissociation rates of Hall & Russo, Camac & Vaughan and Wray. The density profiles calculated using the other values in table 3 are within these limits. The solid lines were calculated using the new oxygen dissociation rate coefficients.

5. Conclusions

Oxygen vibrational and dissociation relaxation has been investigated theoretically and experimentally. Measuring density profiles behind regular reflected shocks by means of laser–differential interferometers has proved to be a good method. This is especially true when the temperature dependence of the relaxation coefficients has to be determined at high temperatures which cannot easily be achieved behind the incident shock. It offers the important advantage of the temperature variation during relaxation being smaller than that encountered behind an incident shock with the same final equilibrium temperature. The relaxation zone behind the oblique reflected shock can be varied by simply changing the wedge angle.

The theoretical model used for the numerical calculations preparing the experiments and for the subsequent evaluations was confirmed by the experiments. In particular, the double-exposure interferograms revealed the regular reflected shocks to be straight even near the reflexion point. The reflexion angle was detected to be larger than that calculated under the hypothesis of flow parallel to the wall. To understand this phenomenon, further theoretical and experimental investigations are necessary. Evaluation of the measured density profiles had to be based upon the measured reflexion angles. In this way the oxygen vibrational relaxation time of Millikan & White could be confirmed and oxygen dissociation rate coefficients could be determined in a new way. The comparison of the new dissociation rates with those previously published by other authors revealed that in particular the new reaction rate coefficient of the O_2–O reaction is significantly smaller.

These new dissociation rates have also been confirmed by recent measurements of the oxygen dissociation relaxation behind stationary oblique shocks using a multibeam laser–differential interferometer. The results are being prepared for publication by Bernzott, Oertel & Schmidt (1976).

The method described may be applied to gases other than oxygen. The results obtained can be used for more precise calculations of vibrational and dissociation relaxation effects in flows of hot gases containing oxygen. The calculations of

regular shock reflexion with and without relaxation have shown that these effects can be quite strong.

The author wishes to express his appreciation to Prof. Dr-Ing. B. Schmidt and Prof. Dr-Ing. J. Zierep for valuable suggestions and stimulating discussions during the investigations. The work was supported from the Deutsche Forschungsgemeinschaft. All numerical calculations have been done with the UNIVAC 1108 of the Rechenzentrum der Universität Karlsruhe.

REFERENCES

ARKHIPOV, V. N. & POLENOV, A. N. 1969 Chemical relaxation in a viscous shock. *Fluid Dyn.* **4** (4), 56.

BERNZOTT, C., OERTEL, H. & SCHMIDT, B. 1976 Oxygen dissociation relaxation behind oblique shocks. To be published.

BLACKMAN, V. H. 1956 Vibration relaxation in oxygen and nitrogen. *J. Fluid Mech.* **1**, 61.

BORTNER, M. H. & GOLDEN, A. 1961 A critique on reaction rate constant involved in the chemical system of high temperature air. *General Elect., R.*, 61 SD0 23 Me 440.

BRADLEY, J. N. 1962 *Shock Waves in Chemistry and Physics.* Wiley.

BRAY, K. N. C. 1959 Atomic recombination in a hypersonic wind tunnel nozzle. *J. Fluid Mech.* **6**, 1.

BYRON, S. R. 1959 Measurement of the rate of dissociation of oxygen. *J. Chem. Phys.* **30**, 6.

CAMAC, M. & FEINBERG, R. M. 1967 *Comb. Inst., Pittsburgh, Pa.*, pp. 137–145.

CAMAC, M. & VAUGHAN, A. 1961 O_2 dissociation rates in O_2–air mixture. *J. Chem. Phys.* **34**, 2460.

CLARKE, J. F. & MCCHESNEY, M. 1964 *The Dynamics of Real Gases.* Butterworths.

GAYDON, A. G. & HURLE, J. R. 1963 *The Shock Tube in High Temperature, Chemical Physics.* New York: Reinhold.

GIBSON, W. E. & BUCKMASTER, J. D. 1964 Effects of species diffusion and heat conduction on nonequilibrium flows behind strong shocks. *A.I.A.A. J.* **2**, 1681.

HALL, J. G. & RUSSO, A. L. 1967 Recent advances in aerothermo-chemistry. *Agard Conf. Proc.* **12**, 443.

JALBERT, P. 1966 Propriétés de l'air à haute température. *Entropie*, **12**, 66.

LANDAU, L. & TELLER, E. 1936 Zur Theorie der Schalldispersion. *Phys. Z.* **10**, 34.

LAW, C. K. 1970 Diffraction of strong shock waves by a sharp compressive corner. *UTIAS Tech. Note*, no. 150.

MAILLIE, F. H. & HSU, C. T. 1968 Relaxation for harmonic and anharmonic oscillators. *A.I.A.A. J.* **6**, 564.

MARTIN, J. J. 1966 *Atmospheric Reentry: An Introduction to its Science and Engineering.* Prentice Hall.

MATHEWS, D. L. 1959 Interferometric measurement in the shock tube of the dissociation rate of oxygen. *Phys. Fluids*, **2**, 170.

MILLIKAN, R. C. & WHITE, D. R. 1963 Systematics of vibrational relaxation. *J. Chem. Phys.* **39**, 3209.

OERTEL, H. 1966 *Stoßrohre.* Springer.

OERTEL, H. JR 1974 Berechnungen und Messungen der Dissoziations-relaxation hinter schief reflektierten Stößen in Sauerstoff. Dissertation, Karlsruhe.

SMEETS, G. & GEORGE, A. 1971 Gasdynamische Untersuchungen im Stoßrohr mit einem hochempfindlichen Laserinterferometer. *ISL-Bericht*, no. 14/71.

SMEETS, G. & GEORGE, A. 1972 Doppelbelichtungs-Interferometrie. *ISL-Bericht*, no. 39/72.

STRICKER, J. & LOW, W. 1972 Atomic oxygen formation times obtained from measurement of electron-density profiles behind shock-waves in air. *Phys. Fluids*, **15**, 2159.

STUPOCHENKO, Y. V., LOSEV, S. A. & OSIPOV, A. I. 1967 *Relaxation in Shock Waves.* Springer.

TAYLOR, D. K. 1966 Theory of the effects of electronic exitation on the vibrational and dissociative relaxation of diatomic molecules. *NOLTR Rep.* no. 256.

VINCENTI, W. G. & KRUGER, C. 1965 *Introduction to Physical Gas Dynamics.* Wiley.

WASSNER, L. 1972 Eindimensionaler und stationärer Verdichtungsstoß unter Berücksichtigung der Transporterscheinungen, der Relaxation der inneren Molekülfreiheitsgrade und der chemischen Reaktionen. *DLR-Forschungsbericht*, no. 72–54.

WECKEN, F. 1968 Daten zur Reaktionskinetik in Luft von 500 °K bis 10000 °K. *ISL Bibliografische Notiz*, D 4/68.

WEIHS, D. & GAL-OR, B. 1972 A new integral–variational method of relaxation regions behind shock and detonation waves. *Israel J. Tech.* **10**, 357.

WETTLAUFER, D. R. 1969 An interferometric determination of the specific refractivities of the nitrogen and oxygen atoms. *UTIAS Tech. Note*, no. 175.

WHITE, D. R. & MILLIKAN, R. C. 1963 Vibrational relaxation of oxygen. *J. Chem. Phys.* **39**, 1803.

WRAY, K. L. 1963 Shock tube study of recombination of O atoms by Ar catalysts at high temperatures. *J. Chem. Phys.* **38**, 1518.

ZEL'DOVICH, Y. B. & RAIZER, Y. P. 1967 *Physics of Shock Waves and High-Temperature Hydrodynamic Phenomena.* Academic.

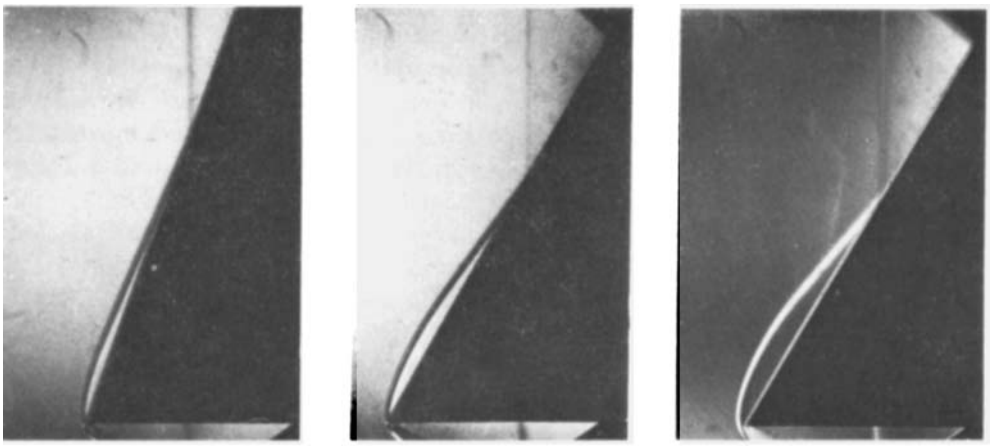

(*a*) (*b*) (*c*)

FIGURE 7. Regular shock reflexion. $p_1 = 133\ \mathrm{N/m^2}$, $T_1 = 295\ ^\circ\mathrm{K}$. (*a*) $M_S = 9{\cdot}2$, $\beta_K = 70^\circ$. (*b*) $M_S = 9{\cdot}2$, $\beta_K = 60^\circ$. (*c*) $M_S = 6{\cdot}5$, $\beta_K = 60^\circ$.

(*Facing p.* 496)